Polymer 50 (2009) 5149–5157

Contents lists available at ScienceDirect

Polymer

journal homepage: www.elsevier.com/locate/polymer

Concentric lamella structures of symmetric diblock copolymers confined in cylindrical nanopores

Shiben Li [a,*], Xianghong Wang [a], Linxi Zhang [a,*], Haojun Liang [a,b], Peng Chen [c]

[a] Department of Physics, Wenzhou University, Wenzhou, Zhejiang 325035, China
[b] Department of Polymer Science and Engineering, University of Science and Technology of China, Hefei, Anhui 230026, China
[c] School of Chemistry, Anhui University, Hefei, Anhui 230039, China

ARTICLE INFO

Article history:
Received 17 May 2009
Received in revised form
9 July 2009
Accepted 4 September 2009
Available online 11 September 2009

Keywords:
Concentric lamella
Diblock copolymer
Cylindrical confinement

ABSTRACT

We applied a real-space self-consistent field theory to investigate the concentric lamella structures of symmetric diblock copolymers confined in the cylindrical nanopores with the preferential surfaces. The symmetric diblock copolymers are selected to locate in the very weak and strong segregation regions where the lamellae obviously exhibit the "soft" and "rigid" characteristics, respectively. For the soft lamellae, the cylindrical confinement induces the soft concentric lamella structure with the same thickness as the bulk lamellar period, except that the thickness of the innermost layer depends on the confinement degree. For the rigid lamellae, the cylindrical confinement not only induces the rigid concentric lamella structure having the linear dependence on the confinement degree, but also results in several novel morphologies, such as the connective concentric lamella and the broken concentric lamella structures. The results are quantitatively discussed in a wide range of confinement degree and can be reasonably understood based on symmetry breaking and structural frustration. In addition, our results are quantitatively compared to the available observations from the simulations and experiments, which are in good agreements and may be helpful to experimentally fabricate the ordered nanostructures on the large scale.

1. Introduction

In order to achieve the delicate balance between the chain stretching energy and the interfacial energy among the block domains, the diblock copolymers can self-assemble into a variety of morphologies in the bulk, ranging from the classical equilibrium structures to the recently reported *Fddd* structures [1–3]. However, the geometric confinements, such as the thin film and the cylindrical nanopore confinements, can break the bulk balance and subsequently induce the novel structures of diblock copolymers through reorienting the commensurability between the confinement surface and the bulk polymer period. An obvious advantage of introducing confinement is that its geometric structure can be used to produce the novel morphologies that are not accessible in the bulk [4]. In general, these confinement-induced structures are on the nanometer length scale, which are of fundamental interests in polymer science and have a great potential for applications in nanotechnology [5–7].

The simplest example of a block copolymer is a symmetrically linear AB diblock copolymer, which exhibits the lamellar morphology in the bulk over a wide range of segregation degree [8,9]. Recently, the symmetric diblock copolymers confined in the cylindrical nanopores are attracting significant interesting in the experimental and theoretical sides, as well as in the computer simulations. It has demonstrated that the symmetry breaking and structural frustration cause a rich variety of microstructures for the symmetric diblock copolymers confined in the cylindrical nanopores. For example, the slab structures have been observed over a wide range of the pore diameter by means of Monte Carlo (MC) simulation when the nanopores have the neutral surfaces [10–12]. Furthermore, the slab structure can be undulated in the pores with the small diameters in the presence of weak preferential surfaces [13]. In these cases, the symmetry of the bulk lamella plays a dominant role in the self-assembly, and the symmetric diblock copolymer exhibits the lamellar structure that maintains the orientation normal to the pore axis. For the moderate degree of the pore diameter, the incommensurability between the pore size and bulk lamellar period results in a series of novel morphologies including the lamellae parallel to the pore axis, helices, catenoid cylinders, and mesh structures [11,12,14–16]. Furthermore, the symmetry of bulk lamella can be completely broken by imposing the strong preferential

* Corresponding authors.
E-mail addresses: shibenli@sohu.com (S. Li), lxzhang@hzcnc.com (L. Zhang).

0032-3861/$ – see front matter © 2009 Elsevier Ltd. All rights reserved.
doi:10.1016/j.polymer.2009.09.011

surface, which requires the lamella to accommodate into a concentric lamella (CL) structure. The symmetric diblock copolymer is a good candidate for observing the CL structures so that the CL structures were observed in the MC simulation for the first time [17], and also in the dynamic density functional theory (DDFT) simulation [10] and the dissipative particle dynamics (DPD) simulation [18]. Subsequently, the CL structures of diblock copolymers were examined in the experiments by the transmission electron microscopy (TEM) [19–21]. Recently, the CL structures were investigated quantitatively by means of MC method, which is in good agreement with the strong-stretching theory (SST) [12,13]. Meanwhile, Li et al. have employed the self-consistent field theory (SCFT) to observe the CL structures where the confined phase diagrams of diblock copolymers were also mapped out [22].

The CL structure not only exists in the diblock copolymer melts, but also appears in the other systems under cylindrical confinements, including the polydisperse diblock copolymers and diblock copolymer mixture melts. For instance, the CL structures (concentric strips) were observed using MC simulation in the polydisperse diblock copolymers under the circle confinement, and the effects of polydispersity index on the CL structures were investigated for the different confinement degrees [23]. Zhu and Jiang reported the CL structures in the $A_{15}B_7/B_7C_{15}$ diblock copolymer mixtures under the cylindrical confinements where the lamella layers are formed with an arrangement sequence of A–B–C–B–A–B–C–B–A as the surfaces prefer to A-blocks [24]. Furthermore, the CL structure can even be observed in the diblock copolymers under the other types of confinements or even in the selective solvents. For the ABC triblock copolymers in selective solvents, when the solvents are selective for the terminal A and C blocks the cylindrical micelles can be observed by atomic-force microscopy (AFM) and TEM [25]. These tubular micelles indeed are similar to the CL structure observed in the diblock copolymer melts. More recently, we preformed an SCFT calculation to investigate the monolayer of CL structure in a periodic array with the small array period and the preferential surfaces [26]. The study revealed that the concentric monolayer is due to the strong cylindrical symmetry originating from either the cylindrical surface field or the cylindrical confinement.

All these studies have demonstrated that the CL structure is an interesting morphology extensively existing in the various polymer systems. However, these previous works mostly concentrate on the qualitative observations on the CL structures by using the experimental and computer simulation's methods. This fact reminds us that further understandings into the characteristics of CL structures are still necessary for the symmetric diblock copolymers. Here, we employed the SCFT calculation method to quantitatively investigate the CL structures of symmetric diblock copolymers under cylindrical confinements in the very weak and the strong segregation regions. Our main purpose is to explore the distinct characteristics of CL structures as well as the novel structures in these special regions over a wide range of pore diameter. The present report is organized as follows. In the next section, we will outline the SCFT calculation method. In the third section, we discuss the CL structures of symmetric diblock copolymers confined in the cylindrical nanopores, in which the CL thicknesses are quantitatively analyzed by the SST and compared to the available observations in the very weak and strong segregation regions. Conclusions are presented in the last section.

2. Calculation method

We consider a system of symmetric diblock copolymers confined in a cylindrical nanopore, having the diameter D and the infinite length at z direction, as shown in Fig. 1a. The n linear AB diblock copolymers are regarded as the Gaussian chains with the same average volume fractions of A- and B-blocks ($f = 0.5$). In the external field, the free energy per chain of diblock copolymers confined in the nanopore with the volume V can be written in the unit of k_BT as follows [27–30],

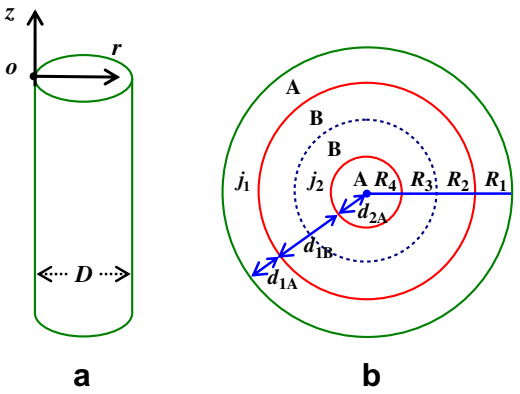

Fig. 1. Sketch map of cylindrical confinement and CL structures. a. The pore with diameter D and infinite length in z direction. b. The concentric lamellae with $n = 2$. The outermost solid circle represents the pore surface, the inside solid circles represent A–B interfaces, and the dashed circles represent the assumed A–A or B–B interfaces in the strong segregation limits. R_i denotes the i-th radius of concentric circle interfaces.

$$\frac{F}{nk_BT} = -\ln\left(\frac{Q}{V}\right) + \frac{1}{V}\int dr[\chi N\phi_A\phi_B - \omega_A\phi_A - \omega_B\phi_B + U_A\phi_A + U_B\phi_B - P(\phi_0 - \phi_A - \phi_B)]. \quad (1)$$

Here, the logarithmic term, $-\ln(Q/V)$, represents the entropic free energy from the chain stretching. The partition function of a single diblock copolymer, Q, can be expressed as, where the propagator, $q(\mathbf{r}, s)$, denotes the probability of any monomers at position, and satisfies a modified diffusion equation,

$$\frac{\partial}{\partial s}q(\mathbf{r}, s) = R_g^2\nabla^2 q(\mathbf{r}, s) - N\omega q(\mathbf{r}, s). \quad (2)$$

with the initial conditions $q(\mathbf{r}, 0) = 1$. Here, R_g is the radius of gyration for an ideal Gaussian chain with the polymerization index N. For the diblock copolymer, when $0 \le s \le f$, $\omega = \omega_A$, otherwise $f < s \le 1$, $\omega = \omega_B$. In most cases, the conjugated propagator $q'(\mathbf{r}, s)$ should be used to express the diffusion from the other end of polymer chain. This conjugated $q'(\mathbf{r}, s)$ satisfies Eq. (2) only with the right-hand side multiplied by -1, and the initial condition, $q'(\mathbf{r}, 1) = q'$. In the present work, we used the Crank–Nicholson scheme to solve the modified diffusion equation, which has been proved to be an efficient for the various confinement boundaries [28–32].

The integral term gives the energies from the block interacting with each other and the external fields. The denotation χN represents the repulsion interaction strengths between two blocks where χ is the Flory–Huggins parameter. The self-consistent fields, $\omega_{A(B)}$, are originated from the repulsion interactions between A- and B-blocks, while $\phi_{A(B)}$ are the monomer density fields normalized by the local volume fractions of blocks. The denotation P is a Lagrange multiplier that ensures the incompressibility of system. Here, we generalize incompressibility constraint to be $\phi_A + \phi_B = \phi_0$, and simplify the form

$$\phi_0(r) = \begin{cases} 0 & r = 0 \quad \text{or} \quad D \\ 0.5 & D > r \ge D - 0.2R_g \quad \text{or} \quad 0 < r \le 0.2R, \\ 1 & D - 0.2R_g > r > 0.2R_g \end{cases} \quad (3)$$

where r is the distance form the pore surface along the radius direction. The strengths of surface preferences, $U_{A(B)}$, are in the unit of χN, reflecting the short-range surface–polymer interactions

between the pore surfaces and $A(B)$ blocks, which have the simple form,

$$U_{A(B)}(r) = \begin{cases} -\eta_{A(B)}\chi N & r = D - 0.2R_g \quad \text{or} \quad r = 0.2R_g \\ 0 & 0.2R_g < r < D - 0.2R_g \end{cases} \tag{4}$$

Here, the coefficients $\eta_{A(B)}$ are non-negative, and represent the reduced strengths of surface adsorption fields.

In order to obtain the equilibrium structure, the free energy of system should be minimized to a stable value. This minimization of free energy results in a set of self-consistent equations under the mean field approximation, and can be expressed as

$$\omega_A(\mathbf{r}) = \chi(\phi_B(\mathbf{r}) - f) + U_A(\mathbf{r}) + P(\mathbf{r}), \tag{5}$$

$$\omega_B(\mathbf{r}) = \chi(\phi_A(\mathbf{r}) - f) + U_B(\mathbf{r}) + P(\mathbf{r}), \tag{6}$$

$$\phi_A(\mathbf{r}) = \frac{V}{Q}\int_0^f ds q(\mathbf{r}, s) q'(\mathbf{r}, s), \tag{7}$$

$$\phi_B(\mathbf{r}) = \frac{V}{Q}\int_f^1 ds q(\mathbf{r}, s) q'(\mathbf{r}, s). \tag{8}$$

These equations can be numerically solved by the combinatorial screening method based on the real-space implementation, originally proposed by Drolet and Fredrickson [28,33]. The real-space implementation is suitable to explore the novel morphologies of copolymers without requiring assumptions of the system symmetry. In the real-space algorithm, an iteration process is assumed to search the equilibrium morphology of copolymers for the given system parameters. The iteration step N_s will stop when the difference between the new free energy and old free energy per chain, that is, the convergence criterion $\Delta F/nk_BT$, reaches to zero. Here, we take criterion being $\Delta F/nk_BT < 10^{-11}$in the calculation process to obtain the final equilibrium states. The SCFT calculations are performed in a PC cluster with 18 nodes, and we take $0.2R_g$ as the lattice size in all calculations, and divide the chain contour length into 200 monomers, which is similar to our previous work [30]. Each minimization of the free energies is run for several times using different random initial mean fields ω_A and ω_B to ensure that the exact equilibrium morphology has been obtained.

In the present study, the segregation parameters of symmetric diblock copolymers are selected to be $\chi N = 15$, $\chi N = 40$ and $\chi N = 120$, locating in the very weak, relatively strong, and very strong segregation regions where they exhibit the very soft, rigid and very rigid lamellae in the bulk, respectively [8,9]. We studied the CL structures of symmetric diblock copolymers confined in both the two-dimensional (2D) and three-dimensional (3D) spaces. The advantage of studying 2D system is that the geometric confinement can be increased to a large size. Since the CL structure has the cylindrical symmetry and is in parallel with the nanopore axis, the 2D morphology can be regarded as the cross sections of 3D morphology, which can provide the basic information about the CL structures such as the lamella thickness. A sketch map of the CL structure in 2D space is shown in Fig. 1b where the $d_{kA(B)}$ denote thicknesses of the A-rich or B-rich layers and k represents the k-th A-rich or B-rich layer. Therefore, we take this advantage to investigate the 2D system in the large confinement size that is not accessible in the 3D space due to the computer capability. Since the diblock copolymers have a rich variety of morphologies in the nanopores [16], we introduce the surface fields with the suitable strengths in order to obtain the CL structures in both the 2D and 3D spaces. For 2D simulation, there is no periodic boundary for the circle confinement in the calculations. However, the periodic boundary condition (PBC) in z direction is selected to construct the infinite length of nanopore in the 3D simulations, as shown in Fig. 1a. The match between the bulk lamellar period and the PBC is crucial to avoid an artifact morphology in a system of infinite size [34–36].

3. Results and discussion

3.1. Soft concentric lamella structures

We select the segregation parameter to be $\chi N = 15$, and investigate the soft CL structures in this section. In order to obtain the CL structures as mentioned above, we introduce the adsorption surface field to the pore surface with the strength of $\eta_A = 0.5$. First, we investigate the CL structures confined in the cylinders with the small diameter of $D = 16.2R_g$ in 3D space in Fig. 2. Then, we discuss the structures confined in the cylinder with the large diameter of $D = 43.2R_g$ and $D = 80R_g$ in Fig. 3, and the dependence of the innermost layer thickness on the pore diameter is quantitatively analyzed in Fig. 4. All these morphologies as well as those in the next section are presented in the form of the red and blue colors, representing the

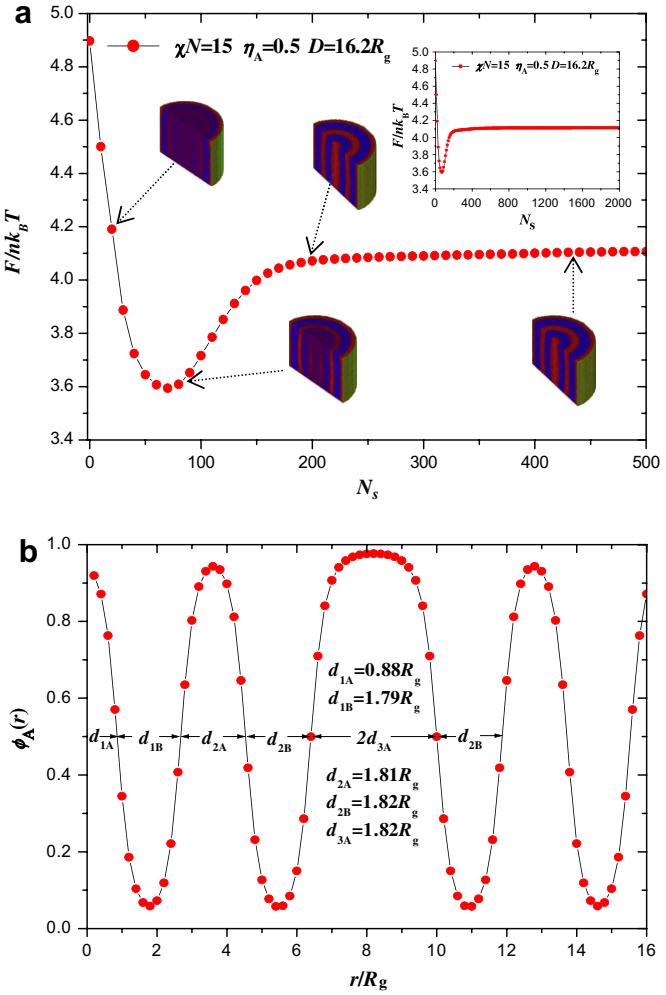

Fig. 2. Example of the soft CL structures confined in the small pore with $D = 16.8R_g$. Here, $\chi N = 15$ and $\eta_A = 0.5$. a. The free energy per chain F/nk_BT as function of iteration step N_s. The morphologies are also inserted in the corresponding positions. b. The monomer density profile $\phi_A(r)$ as function of r, and the corresponding thicknesses are also labeled.

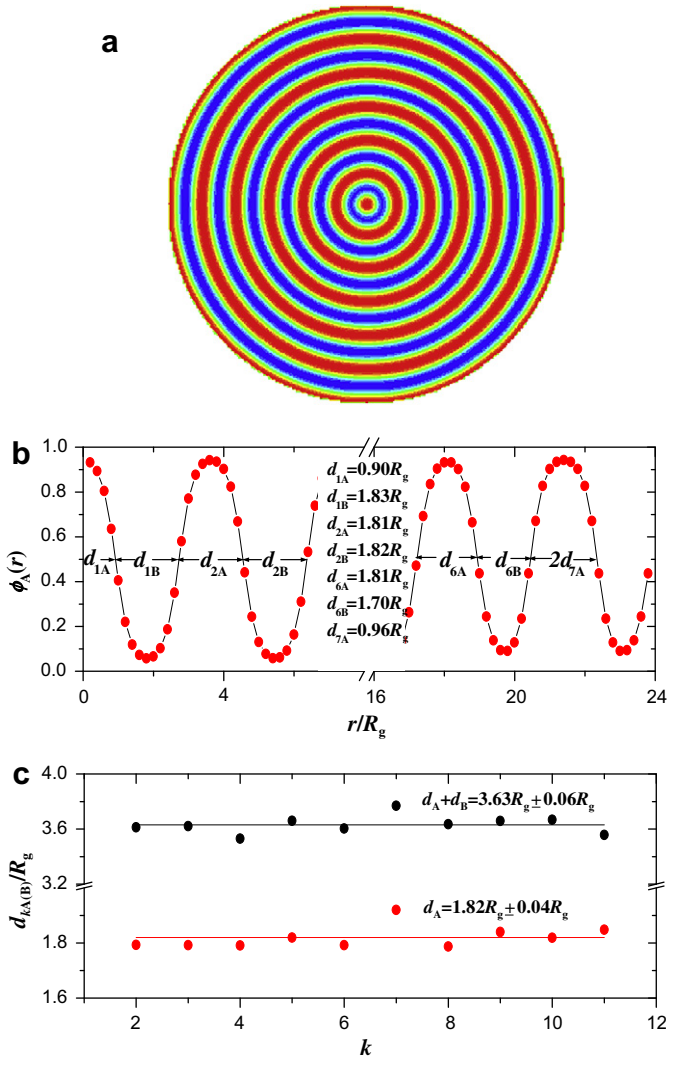

Fig. 3. Example of the soft CL structures confined in the large pore with $D = 43.2R_g$. Here, $\chi N = 15$ and $\eta_A = 0.5$. a. The CL structures with the layer number of $n_L = 6$. b. The monomer density profile $\phi_A(r)$ as function of r, and the corresponding thicknesses domains are also labeled. c. The thickness of the k-th lamella layer for the symmetric diblock copolymer in the large pore with $D = 79.8R_g$.

monomer density distributions belonging to the A- and B-blocks, respectively.

For the pores with small diameters, we obtained the CL structure with the aforementioned system parameters and plotted the free energy F/nk_BT via the iteration step N_s in Fig. 2a to illustrate the evolution process of CL structure, which has been used in the cylindrical phases confined in the thin films [37]. In Fig. 2a, there is an adjustment process until $N_s \approx 200$ because the initial ω_A and ω_B with Gaussian distributions are randomly inputted in the beginning of iteration process. This randomly inputting leads to the decreasing of F/nk_BT in the adjustment process, which is similar to the free energy curves reported for the cylindrical phases confined in thin films [37]. However, this decreasing does not result in the well phase separation structure, as shown in the inserted illustration of Fig. 2a. Meanwhile, the difference between the new and old free energy is so great (namely $\Delta F/nk_BT > 10^{-3}$) that the free energy criterion is not satisfied. Therefore, the free energy with the lowest value is neither a stable nor a meta-stable structure, which is originated from the adjustment for random inputting. Then, there is a convergence process, in which the free energy converges to a stable value, $F_s/nk_BT = 4.113138$, until $\Delta F/nk_BT < 10^{-11}$, and the

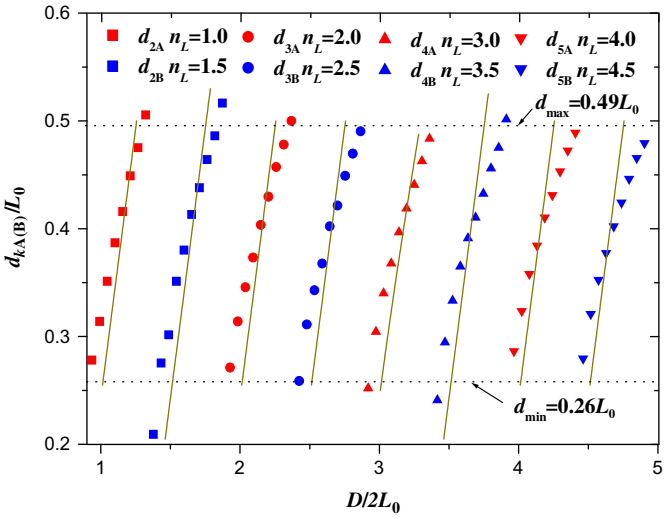

Fig. 4. The innermost layer thickness $d_{kA(B)}$as function of the pore diameter D for the soft CL structures. The discrete dots represent the data from the SCFT calculations, while the solid lines are the resulting from the approximate predictions.

phase is completely separated. In the convergence process, the free energy curve nearly exhibits a planar line, which is also shown in the inserted illustration of Fig. 2a. For the stable equilibrium state, we investigated the monomer density of A-block as function of r, the position along the diameter direction starting from the pore surface, as shown in Fig. 2b. Since the monomer density varies smoothly, the A- and B-blocks mix in a certain domain, indicating that the phase separation is not complete due to the weak repulsion interaction between the blocks. As a consequence, the CL structure is a soft lamella structure [38]. Furthermore, the thickness of A-rich or B-rich layer that defined in Fig. 1b should be obtained by calculating their full wave at half maximum (FWHM), which are labeled in the corresponding positions. These layers are counted starting from the pore surfaces with the thicknesses labeled in Fig. 2b. On the other hand, the bulk lamellar period of $L_0 = 3.63R_g$ can also be obtained by using SCFT calculation method in 2D space, which is in good agreement with the theoretical results [39]. The results show that the outermost layer has the thickness of $L_0/4$ while the inner layers are nearly the same thickness of $L_0/2$. Therefore, we assume that the soft CL structure has the same thickness as the bulk lamellar period except for the outermost and innermost layers.

More detailed data can be provided by the 2D morphologies and confirm this argument in the pores with the large diameters. An example structure confined in the pore with $D = 43.2R_g$ is shown in Fig. 3 where the 2D morphology is exhibited in Fig. 3a and the monomer density profile is plotted in Fig. 3b so that the corresponding thickness can be obtained and labeled. As expected, the results from Fig. 3b confirm the argument that the CL structure has nearly the same thickness as the bulk lamellar period for the large diameter, except for the outermost and innermost layers. Similarly, we further obtained the layer thicknesses in the pore with $D = 80R_g$, and plotted them in Fig. 3c. The black dots are the lamella thicknesses of $d_k = d_{kA} + d_{kB}$, while the red dots represent the thicknesses of A-rich layers d_{kA}. The lines denote the corresponding average values, indicating that the layer thickness is almost a constant, $d_{kA}+d_{kB} = 3.63R_g$ and $d_{kA} = 1.82R_g$, as labeled in Fig. 3c. Actually, we have investigated many cases with the different pore diameters, all of which have the same results. Therefore, we concluded that the outer layer thickness of CL structure is the same as the bulk value in despite of varying the confinement degree. This phenomenon is quite different from the observations on the thin

film confinements. It is true in the thin film confinements that the lamella layers near the film surfaces also have the half thickness of the other layers [27,34,40]. However, the lamellae in the thin film will compress or stretch their layer thickness with $L = D/(n_L+1/2)$ to match the confinement size where n_L denotes the lamella number. For the soft lamellae under cylindrical confinements, the nanopore confinement not only imposes the cylindrical symmetry on the bulk lamella through breaking its natural symmetry, but also reorients the cylindrical symmetry without changing its bulk repeat period. The observations above indicate that the soft CL structure with the same thickness can be induced, which may provide an approach to fabricate these structures on the large size in the experiment.

Although the outer layer has the same thickness, the innermost layer thickness varies as the pore diameter increases. Then, we investigated the innermost layer quantitatively, and plotted the layer thickness as function of pore diameter in step of $0.4R_g$, as shown in Fig. 4. The data extraction method is similar to those in Figs. 2b and 3b where the FWHM denotes the layer thickness. We take the dimensionless parameter $D/2L_0$, that is, a half of the confinement degree, and $d_{kA(B)}/L_0$ as the axes, respectively. First, we observed that the A-blocks and B-blocks appear alternatively in the pore center as the confinement size increases, in despite of the pore surface preferring to the A-blocks. Then, we observed an interesting phenomenon that, for each layer number, n_L, the innermost layer thickness varies almost within the same range. In particular, the thickness is not increased from the zero, but from a fixed average value, $d_{min} = 0.26L_0$. This thickness is equal to the outermost A-block layer, illustrating that they have the similar isolated layer structure. This construct constraints the minimal thickness of the innermost layer, similar to those observed in the thin films [27,34]. On the other hand, the thickness cannot excess the maximal value, the A-rich or B-rich layer thickness, $d_{max} = 0.49L_0$. The conclusion above that the CL structure has the same thickness provides an opportunity to predict approximately the thickness of innermost layers, namely they have a simply linear relationship $d_{kA(B)}/L_0 = D/2L_0 - n_L$. In this approximate prediction, the volume incompressibility can be neglected because the innermost layer occupies only a small space comparing to the outer layers. These relationships are also plotted as the solid lines shown in Fig. 4. In this approximation, the innermost layer thickness increases linearly with the confinement degree, and the predicted results are in good agreement with the calculation results for the severe confinement degrees, namely for $n_L = 1.0$, 1.5, and 2.0, respectively. There are several deviations between the calculation and predicted results in the weak confinement degrees. For the weak confinement degree, the increasing of pore diameter leads to the obvious variation of the confinement space, therefore their influence on the innermost layer thickness can not be neglected in the weak confinement degree case, resulting in the obvious variation.

3.2. Rigid concentric lamella structures

In this section, we first investigate the rigid concentric lamellae with the parameters $\chi N = 40$ and $\eta_A = 0.5$ confined in the nanopores with the small diameter of $D = 17.6R_g$ in the 3D space in Fig. 5, where the effects of surface fields are also discussed. Then, we concentrate on the quantitative analysis for the rigid CL structures with the parameters $\chi N = 120$ and $\eta_A = 1/3$ over a wide range of pore diameter in Fig. 6. In Fig. 7, the phase diagram and novel structures of symmetric diblock copolymers with the parameters of $\chi N = 120$ and $\eta_A = 1/6$ are investigated over a wide range of pore diameter.

For the pores with the small diameters, we plotted the free energy per chain F/nk_BT as function of iteration step N_s in Fig. 5a. The

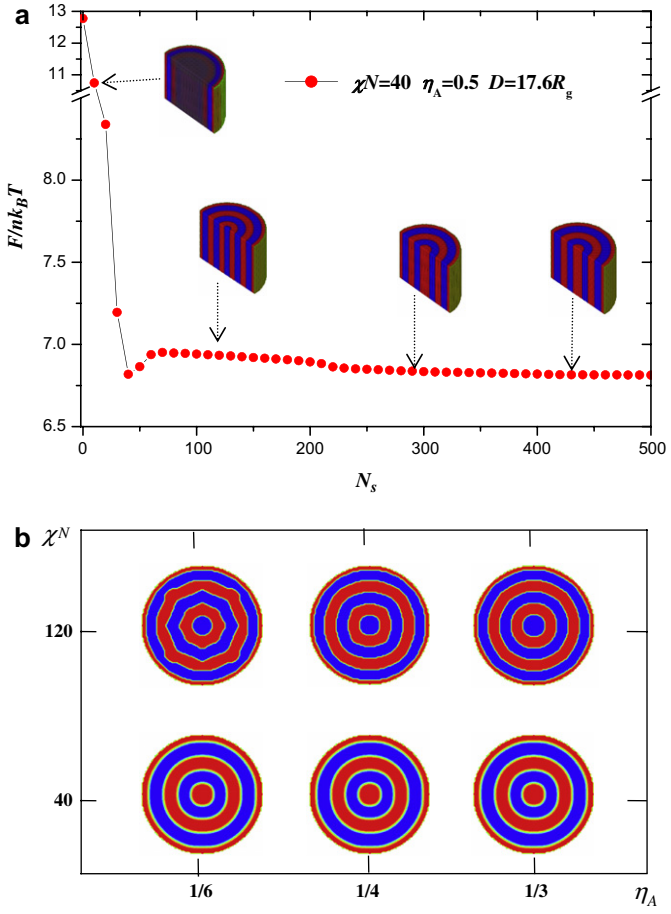

Fig. 5. Example of the rigid CL structures. a. The free energy per chain as function of iteration step with the parameters of $D = 17.6R_g$, $\eta_A = 0.5$ and $\chi N = 40$. b. The effects of surface preferences on the concentric lamellae confined in the pore with $D = 18.8R_g$ for the $\chi N = 40$ and $\chi N = 120$, respectively.

morphologies are also inserted at the corresponding position in the iteration process for handy illustration. Similarly to Fig. 2a, there is also an adjustment process when $N_s < 60$. In this process, the free energy decreases to the lowest value at $N_s = 40$, and then increases

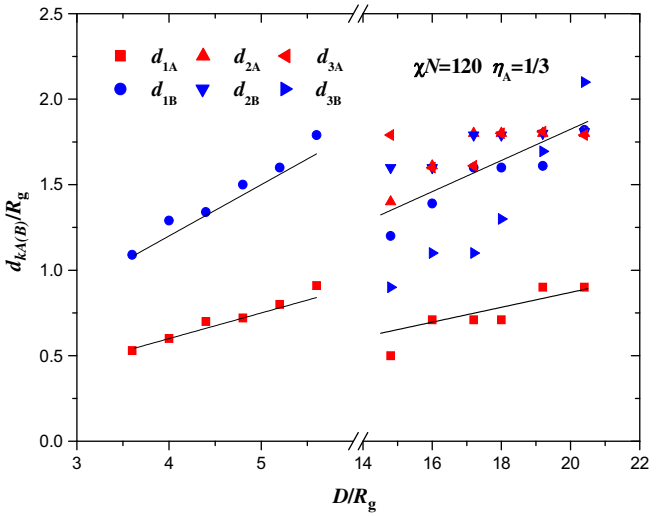

Fig. 6. Comparison of the thicknesses of the rigid CL structures between the SCFT calculations (discrete symbols) and the SST predictions (solid lines) in the strong segregation of $\chi N = 120$ for the $n = 1$ and $n = 5$ cases.

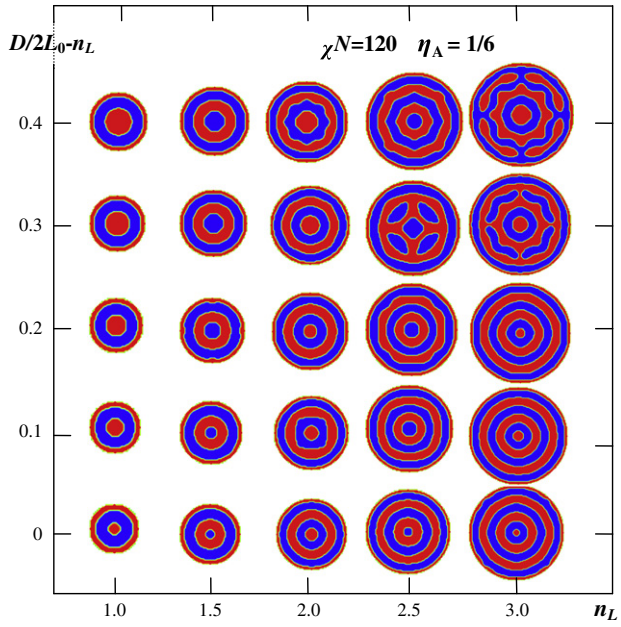

Fig. 7. The phase diagram of rigid lamellae under cylindrical confinements in the strong segregation of $\chi N = 120$. The strength of surface preference is $\eta_A = 1/6$. The phase diagram is arranged as the layer number n_L and the innermost layer thickness $D/2L_0-n_L$. The structures at $D/2L_0-n_L = 3.0$ are minified to about 90 percent of the other structures in size.

until $N_s = 60$.Similarly, the free energy with the lowest value is not a stable structure because of $\Delta F/nk_BT > 10^{-3}$. However, the innermost layer constructed by B-blocks begins to appear at the iteration step of $N_s = 40$. Unlike the case in Fig. 2a, the free energy curve displays a platform at $N_s = 60$–290. In the process of $N_s = 60$–290, the phase is separated and the typical morphology is also inserted in the corresponding position in Fig. 5a where the innermost layer of CL structure is constructed by B-block. Then, the free energy converges to a stable value after $N_s = 290$ until $\Delta F < 10^{-11}$. In the final stable state, the symmetric diblock copolymer has the similar CL structure with the layer number of $n_L = 2$, but the A-block other than the B-block appears in the pore center. From the whole iteration process, we can conclude that the intermediate state appearing at $N_s = 60$–290 is a meta-stable structure. Actually, the meta-stable structures have also been observed for the diblock copolymers confined in the thin films and the nanorod arrays, respectively, by investigating the iteration processes [30,37]. Then, we investigate the dependence of structures on the surface preferences. An example is shown in Fig. 5b where the diblock copolymers are confined in the pores with $D = 18.8R_g$. The CL structure remains unchanged in the segregation of $\chi N = 40$ when the reduced preference strength η_A increases from 1/6 to 1/3. This phenomenon indicates that the structures are not sensitive to the surface preference in the relatively strong segregation. In fact, we have checked all the morphologies with the different pore diameters, and the similar results have been obtained in the segregation of $\chi N = 40$. However, this is not the case in the very strong segregation of $\chi N = 120$. For example, when there is a slight surface preference, the CL structure exhibits somewhat irregular structure, as shown in Fig. 5b. This irregular CL structure will evolve into a prefect CL structure when the strength of surface preference is increased to a suitable value. Therefore, we take this advantage to obtain the very rigid CL structures in the very strong segregation regions.

For the rigid CL structure, the previous SCFT simulation reported that its thickness can be slightly changed as the confinement degree varies [22]. Here, we reported the CL structures in the very strong segregation of $\chi N = 120$. In this special segregation, the very rigid CL structures were obtained by introducing the reduced field strength of $\eta_A = 1/3$, as mentioned above. The SCFT calculation results are shown in Fig. 6 where the $d_{kA(B)}$ represents the thickness of k-th A-or B-rich layer shown in Fig. 1b. Only two cases, the severe and weak confinement cases, were investigated in the 2D space where the discrete symbols denote the SCFT calculation results and the lines are the results from the theoretical predictions.

The theoretical predictions can be done according to the SST [13]. In the strong segregation limit, the A- and B-blocks construct the interfaces labeled as the solid lines in Fig. 1b, which can be numbered by $j = 1,2,\ldots,n$, with $j = 1$ being closest to the pore surfaces. Besides this type of interfaces, the same neighboring blocks can also form another type of interfaces labeled as the dashed lines. These $2n-1$ interfaces together with the pore surface are numbered by $i = 1,2,\ldots,2n$, and form the concentric interfaces with the radius of $R_i (i = 1$being closed to the pore surfaces). Due to the symmetry about the blocks and incompressibility of system, the volume of the $(2j-1)$th layer is equal to that of $(2j)$th layer. Moreover, the interface area per chain is assumed to be constant for the diblock copolymer system [12]. Namely, the area of the (j)th interface is proportional to the total volume of the $(2j-1)$th layer and $(2j)$th layer. Then, the two constraints above can be expressed as

$$R_{2j}^2 - R_{2j+1}^2 = R_{2j-1}^2 - R_{2j}^2, \tag{9}$$

and

$$\frac{R_{2j}^2 - R_{2j+1}^2}{R_{2n}^2} = \frac{R_{2j}}{R_{2n}}. \tag{10}$$

According to these two equations, we can deduce the thickness of A- or B-rich layer, $d_{kA(B)}$, for the any given pore diameter. For example, in the small pore diameter with $n = 1$, the layer thicknesses are

$$d_{1A} = R_1 - R_2 = \left(1 - \frac{\sqrt{2}}{2}\right)\frac{D}{2} \text{ and } d_{1B} = R_2 = \frac{\sqrt{2}}{2}\frac{D}{2}.$$

For the large pore diameter with $n = 5$, we can also deduce the layer thicknesses, which are

$$\begin{aligned} d_{1A} &= R_1 - R_2 = \left(1 - \frac{\sqrt{30}}{6}\right)\frac{D}{2}, \; d_{1B} = R_2 - R_4 \\ &= \frac{\sqrt{30}}{30}\frac{D}{2}, \; d_{2A} = R_4 - R_6 = \frac{\sqrt{30}}{30}\frac{D}{2}, \; d_{2B} = R_6 - R_8 \\ &= \frac{\sqrt{30}}{30}\frac{D}{2}, \; d_{3A} = R_8 - R_{10} = \frac{\sqrt{30}}{30}\frac{D}{2}, \text{ and } d_{3B} = R_{10} \\ &= \frac{\sqrt{30}}{30}\frac{D}{2}. \end{aligned}$$

The prediction results in Fig. 6 indicate that all the layer thicknesses increase linearly with the pore diameters and all the inner layers have the same thicknesses at the $n = 5$case except for the outermost layer. Actually, according to Eqs. (9) and (10), the inner layers with the same thickness can be deduced for an arbitrary given n. The good agreements between the SCFT calculation and SST prediction results are obtained in Fig. 6, especially for the $n = 1$ case. Since the outermost A-rich layer is constructed by an isolated layer whereas the inner A- or B-rich layer consists of two layer as mentioned before, its thickness is always much smaller than those of the inner layers. Moreover, the excellent agreements between the simulation results and theoretical predictions have been obtained for the outermost layer because their largest diameter decreases the errors for the simulation results. The difference between the symbols and

the corresponding lines for $d_{3A(B)}$ indicates that the cylindrical confinement lead to the deviations of interface areas from those of bulk values. In contrary to the outermost layer, the thickness of the innermost A- or B-rich layer is always much larger than that of the outermost layer, thought it is also an isolated layer. This is because of the fact that the innermost layer is actually a solid cylinder with small diameter and the incompressibility of copolymer requires its larger diameter.

The prefect rigid concentric lamellae may vanish when the surface preference decreases to a certain degree, as shown in Fig. 5b. This phenomenon activates us to explore the novel structures in the strong segregation region of $\chi N = 120$. Here, we investigate the morphologies of symmetric diblock copolymers confined in the pores with the surface preferences of $\eta_A = 1/6$. We plotted the phase diagram in Fig. 7 that arranged as the lamella number n_L and the innermost layer thickness $D/2L_0 - n_L$. We take the advantage of this arrangement to discuss the structural characteristic in two sides. On one hand, due to the severe cylindrical confinement, although the bulk lamella has a good rigidity, the strong cylindrical symmetry originating from the severe confinement still break the natural symmetry of bulk lamella in the small space. Therefore, it is not surprising that the perfect CL structures appear in cases of the small given values of $n_L = 1.0$ and 1.5. When the lamella number is increased to be $n_L = 2.0$, the cylindrical symmetry still requires the outermost lamella layer to suit the cylindrical structure, while the inner layers exhibit the natural symmetry of bulk lamella because of the weak cylindrical symmetry in the inner area. Thus, these layers exhibit several flat characteristic similar to the bulk lamellae. As the pore diameter increases continuously, the more space leave to form the layers, and more complex structures appear in the pores with large diameters. For example, we observed a connective CL structure at $n_L = 2.5$ and $D/2L_0 - n_L = 0.3$ where its neighboring layers connect with each other. For this large pore diameter, the symmetry of bulk lamella is only partly broken due to the weak surface preference so that the bulk lamella symmetry dominates in the inner zone of pore. The bulk lamella symmetry requires the flat characteristic along the x and y axes, and breaks the axial symmetry. However, the connection between the neighboring layers break at a suitable value of $n_L = 2.5$ and $D/2L_0 - n_L = 0.4$, and the confined diblock copolymer exhibits an unperfect CL structure with several flat characteristics, as shown in Fig. 7. This disconnection is probably due to the greater spacing between the neighboring layers at the point of (2.5, 0.4) than that at the point of (2.5, 0.4). As a result, the (2.5, 0.3) point breaks the axial symmetry more obviously than the (2.5, 0.4) point. Similar phenomenon were observed for $n_L = 3.0$ where the breaking of axial symmetry occurs at the points of (3.0, 0.3) other than the points of (3.0, 0.4). By comparing the connective structures at $n_L = 2.5$ and 3.0, the difference is that the connection between the neighboring layers is more weak at the (3.0, 0.3) point than those at the (2.5, 0.3) point due to the greater spacing of in the greater spacing between the neighboring layers at the point of (3.0, 0.3). On the other hand, at the given $D/2L_0 - n_L$, the innermost A- or B-rich layer appears alternatively in the pore center, similarly to the soft CL structures. For $D/2L_0 - n_L = 0$, the morphologies are almost the prefect CL structures that are independence with the layer number n_L. Under this condition, the confinement size is commensurate with the bulk lamella period, only the cylindrical symmetry constrains the formation of structure, which requires the appearance of the CL structures. However, when the confinement size is severely incommensurate with the bulk lamella period, the structural frustration can be observed for the CL structures. For instance, the broken CL structure appears at $n_L = 3.0$ and $D/2L_0 - n_L = 0.4$, similarly to a club structure with the broken layers. Based on the analysis above, we concluded that both the structural frustrations and the symmetry breaking lead to the complex structures appearing in the phase diagram of symmetric diblock copolymers in the very strong segregation regions. In addition, we have checked the free energy curves for all the structures in this phase diagram. We observed that all the evolution processes can be also divided into the adjustment and convergence processes, similar to the curve observed in Fig. 2a. Therefore, we didn't observe the meta-stable structures in this phase diagram although they have complexly stable structure.

3.3. Comparison to the available observations

On the simulation's side, we would like to make some comparison to the MC and DDFT observations. A direct comparison between the MC (DDFT) and SCFT results is complicated because their system parameters are different. A symmetric A_5B_5 diblock copolymer has been investigated in the MC simulation where the interaction between the different blocks ε_{AB} is set to be $\varepsilon_{AB} = 0.3k_BT$ [14]. According to the expression for the bond fluctuation model [41], $\chi \approx 5(\varepsilon_{AB}/k_BT)$, we recalculated the parameter used in Ref. [14] is to be $\chi N \approx 15$, which is located in the weak segregation region. In their study, the attractive interactions between the A blocks and the pore surfaces ε_{AS} is varied and the circle lamellae (that is, the CL structures) have been observed at $\varepsilon_{AS} > 0.14k_BT$ and $D/L_0 = 1.5-3.1$. These MC results confirm our SCFT observations for the soft CL structures with the parameters of $\chi N = 15$, $\eta_A = 0.50$and $D/L_0 = 2.0-10.0$. In the DDFT calculation, a A_8B_8 diblock copolymer was considered for $\varepsilon_{AB} = 2.5kJ/mol$ and various ε_{AS}[10]. According to the expression of $\chi_{AB} = 1000\varepsilon_{AB}/8.31T$ (with $T = 300$) [16], we deduced that the model copolymer adopted in Ref.10 is located in the weak segregation of $\chi N \approx 16$. In this DDFT study, the dartboard morphology (that is, the CL structure) has been observed at the moderate degree of surface field strength, indifferent to the pore diameter. This result further confirms that our SCFT observations on Figs. 2–4 are the CL structures with the aforementioned parameters.

For the innermost layers of soft CL structures, the DDFT study has observed the alternative appearance of distinct blocks in the pore center for the different radii of 8, 14, and 24, which is in accordance to the $n_L = 2$, 3 and 4, respectively [10]. The MC simulation study has observed this alternative appearance for the soft structures where the pore diameter is at the range of $d/L_0 = 1.5-3.1$ [14]. Furthermore, both the MC and DDFT studies reported that the outermost layer thickness holds $d_1 \approx L_0/4$, which are in good agreement with our SCFT predictions in the weak segregation [10,14]. However, there are unavailable simulation data to compare with our SCFT observations on Figs. 3 and 4 in detail, instead of approximately quantitative comparisons.

For the rigid CL structures, Chen et al. have performed a MC study on the $A_{10}B_{10}$ diblock copolymer with $\varepsilon_{AB} = 1.0k_BT$ to investigate the surface field effects. We recalculated the segregation degree to be $\chi N = 100$ in their study, locating in the strong segregation region. For a given surface field strength of $\varepsilon_{AS} = 0.40k_BT$, they observed the cylinder barrels with alternative block domains in the pore center for the pore radii $R = 16$, 22, and 26, respectively. This result is in agreement with our SCFT observations on Fig. 5 where it provides more detailed data. Actually, the alternative domains have also been observed in the $A_{12}B_{12}$ model with $\varepsilon_{AB} = 1/2.3k_BT$ and A_6B_6 model with $\varepsilon_{AB} = 1.0k_BT$ [12,13], in which the diblock copolymers are located in the relatively strong segregations of $\chi N = 52$ and 60, respectively. Their results show that the order parameter varies from -1 (represent the pure B block) to 1 (represent the pure A block) as the pore diameter increases from $1.5L_0$to about $2.5L_0$. These results are consistent with our observations on the rigid CL structures quantitatively analyzed in Figs. 6 and 7. Moreover, the MC simulation also reported that the

outermost layer thickness obeys $d_1 \approx L_0/4$ for the outermost layer [12], which is also in agreement with our SCFT observations.

Up to now, there are unavailable data to be compared for the linear variations of the layer thickness for the symmetric diblock copolymers in the very strong segregation of $\chi N = 120$. Fortunately, Li's and Wang's groups have investigated the variations of the layer thickness for the symmetric diblock copolymers in the segregations of 52 and 60, respectively [12,13]. In their studies, the authors reported the MC results for the $n = 1$–3 cases, which were compared to the SST predictions. Our SCFT results indicate that the layer thickness depends on the diameters, namely, $d_{1A} = (1 - \sqrt{2}/2)\frac{D}{2}$ and $d_{1B} = \frac{\sqrt{2}}{2}\frac{D}{2}$ for the $n = 1$ case. Therefore, our SCFT results are not only in good agreement with the MC results, but also consistent with the SST predictions. For the large pore diameters with $n = 5$, there are not available MC and DDFT simulation results to be compared for the large case so that our predicted SCFT results are only compared to the SST ones in the present work, which are also in general agreement.

In the experimental side, Russell's group have reported the CL structures of symmetric diblock copolymers where the PS-*b*-PBD are confined in the alumina membranes preferring to the PBD blocks [19,20]. Using the earlier measurements by the same group [42], $\chi = \chi_S + \chi_H/T$ (χ_S and χ_H refer to the entropic and enthalpic contributions, respectively), we estimated the parameters of $\chi = 0.058$ and $N \approx 250$. Therefore, the diblock copolymers they used are located in the weak segregation of $\chi N \approx 14.5$. In their study, the CL structures with $n_L = 2$–4 have been observed in the commercial membranes with the diameters from 100 nm to 350 nm, and the TEM images show that the PBD and PS domains appear alternatively in the pore center. They observed that the increasing of the layer number is not continuous as the pore diameter increase, and the CL thickness is varied with the pore diameters. These observations are in accordance with our SCFT results for the soft CL structures where the layer thickness has the nearly linear dependence on the pore diameter. Moreover, Sun et al. have observed the CL structures in the alumina pore in the symmetric diblock copolymer (PS-*b*-PMMA) system with the polymerization index of $N \approx 680$ [21]. According to the expression of $\chi = 0.0294 + 3.2/T$ [43], we recalculated the segregation degree of $\chi N \approx 24.8$at $T = 453.13$, indicating that the PS-*b*-PMMA diblock copolymers are located in the weak segregation. In their experiment, the overall number of CL structures increases and the PS and PMMA domains appear alternatively in the pore center when the pore diameter is varied from 25 nm to 400 nm. These experimental observations further confirm our SCFT predications on the soft CL structures.

In the strong segregation, it is still not available experimental data to compare for the CL structures and other novel SCFT predicted structures, such as the connective CL structure. It is suggested that these novel structures should be observed by controlling the temperature and pore size to a certain value in the experiment. Generally, in order to reach the strong segregation, the diblock copolymers require the large polymerization index N and the Flory–Huggins parameter χ. Therefore, the diblock copolymers with high molecular weight are necessary to anneal to a low temperature in order to observe the rigid CL structures or novel structures in the experiment.

4. Conclusion

We have performed both the 2D and 3D SCFT calculations for the concentric lamella structures of symmetric diblock copolymers confined in the nanopores. The soft and rigid CL structures have been systematically studied by investigating the monomer density profiles, the free energies and the morphologies. By varying the confinement degree over a wide range, several distinct characteristics of soft and rigid CL structures have been quantitatively discussed in detail, and the novel structures have been predicted for the symmetric diblock copolymers in the special segregation regions.

For the soft lamellae, it is easy to break the natural symmetry of bulk lamellae and accommodate the cylindrical symmetry. For the outer layers, we confirmed that, besides the outermost layer, these layers have the same thicknesses as the bulk period, which are independent in the confinement degree. However, we observed that the A- and B-block domains appear alternatively at the pore centers, and obtained the nearly linear dependence of the innermost layer thickness on the confinement degree where the innermost layer thickness varies within a fixed range. Furthermore, we have done a simple quantitative analysis for the innermost layer thickness, and the general agreements have been obtained for the soft CL structure. We discussed these characteristics of soft CL structures by comparing to the lamellae confined in the thin films, where the different morphological behaviors were concluded to be the different symmetries from their geometric confinements. For the rigid lamella, the SCFT results indicate that the layer thickness of CL structure varies linearly with the confinement degree. On the other hand, the layer thickness has also been quantitatively analyzed by the SST, which is consistent with the SCFT results. Moreover, the phase diagram arranged as the layer number and thickness of the innermost layer has been discussed in the weak surface preference for the special segregations. Several novel morphologies, such as the connective CL and the broken CL structures, have been observed in the phase diagram where their characteristics have been discussed in detail, and can be understood based on the symmetry breaking originating from the cylindrical confinement and the structural frustration between the lamella period and confinement size.

The results indicate that the soft and rigid lamellae have the distinct morphological behaviors under cylindrical confinement, especially for their different variations on the thicknesses. The symmetry can be easy to break for the soft lamellae due to their relative weak natural symmetry whereas the rigid lamellae exhibit the strong natural symmetry that is difficult to break, especially in the pore center. Our results were also quantitatively compared to the available results from the MC and DDFT simulations and the general agreements were obtained in the weak and strong segregations. Moreover, our SCFT predictions are in accordance with the experimental results in the weak segregation, and suggested that the rigid CL structures and novel structures should be examined in the diblock copolymers with the high molecular weight at a low temperature. Our quantitative results for the soft and rigid CL structures should be useful as designing the polymer nanomaterials.

Acknowledgment

This research was supported by the General Program of National Natural Science Foundation of China (Nos. 20574052, 20374050, 20490220, 90403022 and 20804001), the Outstanding Youth Fund of China (No.20525416), the National Basic Research Program of China (No.2005CB623800), Program for New Century Excellent Talents in University (NCET-05-0538) and Natural Science Foundation of Zhejiang Province (Nos.R404047, Y405011, Y405553). The authors thank the referees for their critical reading of the manuscript and their very good ideas.

References

[1] Tyler CA, Morse DC. Phys Rev Lett 2005;94:208302.
[2] Takenaka M, Wakada T, Akasaka S, Nishitsuji S, Saijo K, Shimizu H, et al. Macromolecules 2007;40:4399.

[3] Kim MI, Wakada T, Akasaka S, Nishitsuji S, Saijo K, Hasegawa H, et al. Macromolecules 2008;41:7667.
[4] Yu B, Sun P, Chen T, Jin Q, Ding D, Li B, et al. Phys Rev Lett 2006;96:138306.
[5] Krausch G, Magerle R. Adv Mater 2002;14:1579.
[6] Park C, Yoon J, Thomas EL. Polymer 2003;44:6725.
[7] Wu Y, Cheng G, Katsov K, Sides S, Wang J, Tang J, et al. Nat Mater 2004;3:816.
[8] Matsen MW, Schick M. Phys Rev Lett 1994;72:2660.
[9] Matsen MW, Bates FS. Macromolecules 1996;29:1091.
[10] Sevink GJA, Zvelindosky AV, Fraaije JGEM, Huinink HP. J Chem Phys 2001;115:8226.
[11] Chen P, He X, Liang H. J Chem Phys 2006;124:104906.
[12] Yu B, Sun P, Chen T, Jin Q, Ding D, Li B, et al. J Chem Phys 2007;127:114906.
[13] Wang Q. J Chem Phys 2007;126:024903.
[14] Feng J, Ruckenstein E. Macromolecules 2006;39:4899.
[15] Feng J, Ruckenstein E. J Chem Phys 2006;125:164911.
[16] Sevink GJA, Zvelindovsky AV. J Chem Phys 2008;128:084901.
[17] He X, Song M, Liang H, Pan C. J Chem Phys 2001;114:10510.
[18] Feng J, Liu H, Hu Y. Macromol Theory Simul 2006;15:674.
[19] Shin K, Xiang H, Moon SI, Kim T, McCarthy TJ, Russell TP. Science 2004;306:76.
[20] Xiang H, Shin K, Kim T, Moon SI, McCarthy TJ, Russell TP. Macromolecules 2004;37:5660.
[21] Sun Y, Steinhart M, Zschech D, Adhikari R, Michler GH, Gosele U. Macromol Rapid Commun 2005;26:369.
[22] Li W, Wickham RA, Garbary RA. J Chem Phys 2006;39:806.
[23] Han Y, Cui J, Jiang W. Macromolecules 2008;41:6239.
[24] Zhu Y, Jiang W. Macromolecules 2007;40:2872.
[25] Njikang G, Han D, Wang J, Liu G. Macromolecules 2008;41:5697.
[26] Li S, Chen P, Wang X, Zhang L, Liang H. J Chem Phys 2009;130:014902.
[27] Matsen MW. J Chem Phys 1997;106:7781.
[28] Drolet F, Fredrickson GH. Phys Rev Lett 1999;83:4317.
[29] Yang S, Yan D, Shi A-C. Macromolecules 2006;39:4168.
[30] Chen P, Liang H, Shi A-C. Macromolecules 2007;40:7329.
[31] Tang P, Qiu F, Zhang H, Yang Y. Phys Rev E 2004;69:031803.
[32] Chen P, Liang H, Shi A-C. Macromolecules 2008;41:8938.
[33] Fredrickson GH, Ganesan V, Dorlet F. Macromolecules 2002;35:16.
[34] Wang Q, Yan Q, Nealey PF, de Pablo JJ. J Chem Phys 2000;112:450.
[35] Wang Q, Nealey PF, de Pablo JJ. Macromolecules 2001;34:3458.
[36] Larson RG. Macromolecules 1994;27:4198.
[37] Heckmann M, Drossel B. Macromolecules 2008;41:7679.
[38] Wang Q, Nealey PF, de Pablo JJ. Macromolecules 2002;35:9563.
[39] Wang Q. J Chem Phys 2008;129:054904.
[40] Kellogg GJ, Walton DG, Mayes AM, Lambooy P, Russell TP, Gallagher PD, et al. Phys Rev Lett 1996;76:2503.
[41] Freire JJ, McBride C. Macromol Theory Simul 2003;12:237.
[42] Owens JN, Gancarz IS, Koberstein JT, Russell TP. Macromolecules 1989;22:3380.
[43] Wang J-Y, Chen W, Russell TP. Macromolecules 2008;41:4904.